

THE OBSERVATIONAL MASS FUNCTION OF NEARBY GALAXY CLUSTERS

MARISA GIRARDI^{1,2}, STEFANO BORGANI³, GIULIANO GIURICIN², FABIO MARDIROSSIAN^{1,2},
AND MARINO MEZZETTI²¹Osservatorio Astronomico di Trieste, Via Tiepolo 11, I-34131 Trieste, Italy²SISSA, via Beirut 4, I-34014 Trieste, Italy; and Dipartimento di Astronomia, Università degli Studi di Trieste, Trieste, Italy

E-mail: girardi, giuricin, mardiros, mezzetti @sissa.it

³INFN, Sezione di Perugia, c/o Dipartimento di Fisica dell'Università,
via A. Pascoli, I-06123 Perugia, Italy; E-mail: borgani@perugia.infn.it

ABSTRACT

We present a new determination of the mass function of galaxy clusters, based on optical virial mass estimates for a large sample of 152 nearby ($z \leq 0.15$) Abell-ACO clusters, as provided by Girardi et al. (1998). This sample includes both data from the literature and the new ENACS data. The resulting mass function is reliably estimated for masses larger than $M_{lim} \simeq 4 \times 10^{14} h^{-1} M_{\odot}$, while it is affected by sample incompleteness at smaller masses.

We find $N(> M_{lim}) = (6.3 \pm 1.2) 10^{-6} (h^{-1} Mpc)^{-3}$ for cluster masses estimated within a $1.5 h^{-1} Mpc$ radius. Our mass function is intermediate between the two previous estimates by Bahcall & Cen (1993) and by Biviano et al. (1993).

Based on the Press-Schechter approach, we use this mass function to constrain the amplitude of the fluctuation power spectrum at the cluster scale. After suitably convolving the PS predictions with observational errors on cluster masses and *COBE*-normalizing the fluctuation power spectrum, we find $\sigma_8 = (0.60 \pm 0.04) \Omega_0^{-0.46+0.09\Omega_0}$ for flat low-density models and $\sigma_8 = (0.60 \pm 0.04) \Omega_0^{-0.48+0.17\Omega_0}$ for open models (at the 90% c.l.).

Subject headings: galaxies: clusters: general - cosmology: observations - cosmology: theory - large scale structure of universe.

1 INTRODUCTION

According to the scenario of hierarchical formation of cosmic structures, clusters of galaxies arise from rare high peaks of the initial density fluctuation field and, at present time, represent the largest virialized cosmic structures. As a consequence, standard analytical arguments based on the Press & Schechter (1974; hereafter PS) approach show that their abundance is highly sensitive to the amplitude of the density fluctuations on the cluster mass scale (e.g., White, Efstathiou & Frenk 1993). In particular, if M is the typical cluster mass and Ω_0 is the cosmic density parameter, then the typical size of the density fluctuation collapsing into a cluster is $R \propto (\Omega_0 M)^{1/3}$. Typical cluster masses, $M \sim 5 \times 10^{14} h^{-1} M_{\odot}$ ¹, are rather close to the average mass contained within a sphere of $8h^{-1} Mpc$ radius. Therefore, it is common to express constraints from the observed local cluster mass function (i.e., the number density of clusters of a given mass), $n(M)$, in terms of Ω_0 and σ_8 , the r.m.s. density fluctuation within a sphere of $8h^{-1} Mpc$ radius (e.g., Eke, Cole, & Frenk 1996; Viana & Liddle 1996).

From the theoretical side, the mass function of clusters is easily obtainable either from N-body simulations or, to a comparable degree of reliability (e.g., Lacey & Cole 1993; Eke et al. 1996; Borgani et al. 1998), by applying the analytical PS recipe. On the contrary, predictions of cosmological models about quantities which are more directly connected to observations, like the internal velocity

dispersion of member galaxies, σ_v , and the X -ray temperature of the intracluster gas, T_X , are much less straightforward and rely on assumptions which are quite debated. As for σ_v , N-body simulations allow reliable predictions of the internal velocity dispersion of clusters, but only for the DM particles (e.g., Frenk et al. 1990; Borgani et al. 1997; van Haarlem, Frenk, & White 1997), while the connection to the observed σ_v requires a plausible model of galaxy formation. Numerical simulations by Frenk et al. (1996) have shown that present uncertainties about the physics of galaxy formation in clusters can lead to an incorrect determination of the virial mass by up to a factor five. As for T_X , it is generally believed to be a rather accurate indicator of the cluster mass (e.g., Evrard, Metzler, & Navarro 1996). On the other hand, both analytical predictions and hydrodynamical cluster simulations, based only on the adiabatic physics of the intracluster gas, are able to reproduce neither the observed relation between bolometric X -ray luminosity and temperature (e.g., Eke, Navarro & Frenk 1997; Bryan & Norman 1998, and references therein), nor the observed size of core radii in the gas distribution (e.g., Makino, Sasaki, & Suto 1998, and references therein). Such a discrepancy creates a need to introduce additional physics to explain the thermodynamics of the intra-cluster gas (e.g., Bower 1997; Cavaliere, Menci, & Tozzi 1997, and references therein).

From the observational side, cluster masses are inferred from either X -ray or optical data, under the general hypothesis of dynamical equilibrium. Estimates based on

¹Here h is the Hubble constant in units of $100 \text{ km s}^{-1} \text{Mpc}^{-1}$

gravitational lensing do not require assumptions about the dynamical status of the cluster, but a good knowledge of the geometry of the potential well is necessary (e.g., Narayan & Bartelmann 1997). Claims for a discrepancy (by a factor 2-3) between cluster masses obtained with different methods casted doubts about the general reliability of mass estimates (e.g., Wu & Fang 1997). However, recent analyses have shown that such discrepancies can be explained by the different way in which strong cluster substructures bias mass estimates based on different methods (Allen 1997; Girardi et al. 1997). In particular, the analysis by Girardi et al. (1998, hereafter G98) demonstrated that, for nearby clusters without strong substructures, a good overall agreement exists between X -ray and optical virial mass estimates.

A reliable determination of cluster masses is a necessary but not sufficient condition to guarantee a reliable estimate of the mass function. Indeed, the latter also requires a cluster sample which is large enough to be a fair representation of the cluster population in the local Universe, at least above a certain mass limit. In past years, such requirements limited the possibility of obtaining a stable result about the cluster mass function and, in fact, the only two estimates so far presented (Bahcall & Cen 1993, hereafter BC93; Biviano et al. 1993, hereafter B93) turn out to be quite discrepant. BC93 derived cluster masses by using global scaling relations to connect mass to cluster richness and X -ray temperature. B93 estimated cluster masses from a homogeneous virial analysis of about 70 clusters and found a larger abundance, by about one order of magnitude, at the mass scale $M \simeq 5 \times 10^{14} h^{-1} M_\odot$ (cf. also Figure 3 below).

A new and more robust determination of the observational mass function based on optical virial analysis is now possible thanks to the recent availability of a large amount of redshift data for rich clusters, as provided by the ESO Nearby Abell Cluster Survey (ENACS; Katgert et al. 1996; 1998). Recently, G98 computed virial masses in a homogeneous way for a large sample of ~ 170 clusters, obtained by combining the ENACS sample with data from other authors (see also Fadda et al. 1996; hereafter F96). The extension of this sample makes it the largest available data set over which to reliably estimate the cluster mass function.

In the following analysis we will use the G98 results with the twofold aim of (*a*) estimating the optical virial mass function of nearby galaxy clusters, and (*b*) investigating the subsequent constraints on the power spectrum of cosmic density fluctuations.

This paper is organized as follows. In § 2 we briefly describe the statistical sample of clusters masses as obtained by G98 and then present the determination of the cluster mass function. Afterwards, we compare it with previous determinations based on optical data by BC93 and B93. In § 3 we apply the PS approach to place constraints on the fluctuation power spectrum for different cosmological models. We give a brief summary of our main results and draw our conclusions in § 4.

2 THE DETERMINATION OF THE MASS FUNCTION

2.1 *The Statistical Sample of Cluster Masses*

In the following analysis we largely use the results by G98, who analyzed optical data (galaxy positions and velocities) for 170 nearby clusters having $z \leq 0.15$. The original optical data partly comes from the literature and partly from the ENACS dataset (Katgert et al. 1996; 1998). In this section we summarize the G98 results which are relevant for the mass function analysis and we refer to that paper for further details.

The total mass of each cluster is computed by applying the virial theorem to the member galaxies, under the usual assumption that the mass distribution follows the galaxy distribution (e.g., Limber & Mathews 1960; Giuricin, Mardirossian, & Mezzetti 1982; Merritt 1988; B93). This assumption is supported by several pieces of observational evidence, coming both from optical (e.g., Carlberg, Yee, & Ellingson 1997) and X-ray data (e.g., Watt et al. 1992; Durret et al. 1994; Cirimele, Nesci, & Trevese 1997), as well as from gravitational lensing data (e.g., Narayan & Bartelmann 1997). Although some level of uncertainty still remains about the very central cluster regions, detailed optical analyses (Cirimele et al. 1997; see also Merritt & Tremblay 1994 for the Coma cluster) suggest a very peaked galaxy distribution, in agreement with data on the dark matter distribution from gravitational lensing (see, e.g., Narayan & Bartelmann 1997).

In order to fit the galaxy distribution for each cluster, G98 used a King-like profile, $\rho(r) \propto (1 + r^2/r_c^2)^{-3\beta/2}$, where r_c is the core radius and β is a free exponent. They found that, on average, $\rho(r) \propto r^{-2.4}$ for the scaling of the galaxy number density in the outer part of the clusters, thus in agreement with previous studies (e.g., Bahcall & Lubin 1994; Girardi et al. 1995), with a peaked distribution in the inner part ($r_c \sim 50 h^{-1} \text{kpc}$; see also § 8 of G98).

G98 computed cluster masses within the radius $0.002 \cdot \sigma_v h^{-1} \text{Mpc}$, that represents a rough estimate of the virialization radius R_{vir} , within which dynamical equilibrium is expected to hold. A surface term correction has also been applied to the usual virial mass estimator which, otherwise, would have overestimated the true cluster mass (e.g., The & White 1976; Binney & Tremaine 1987; Carlberg et al. 1997b). This correction amounts to 19%, very similar to that suggested by Carlberg et al. (1997b) for CNO clusters.

G98 compared their optical mass estimates to those derived from X -ray analyses for a list of 66 clusters, which they compiled from the literature, and found an overall good agreement (cf. Figure 5 of G98). This agreement is expected in the framework of the two assumptions that mass follows the galaxy distribution and that clusters are not far from dynamical equilibrium (see also Evrard et al. 1996; Schindler 1996; Carlberg et al. 1997c). Only about

10% of clusters show at least two strongly superimposed peaks in their velocity distribution thus indicating that they probably are far from dynamical equilibrium. The ambiguity in the treatment of these clusters – peaks can be treated as either disjoined or joined into a single structure – leads to mass estimates which differ by a factor ~ 3 on average (cf. § 6 of G98). The effect of these clusters with uncertain dynamics in the estimate of the mass function will be discussed in the following.

As a concluding remark, we point out that the size of our sample, along with the overall good agreement between X -ray and optical cluster masses, makes it the largest available data set over which to reliably estimate the cluster mass function.

2.2 From Masses to the Mass Function

The results from G98 that we will use in our analysis of the cluster mass function are the following: (i) the values of the (line-of-sight) velocity dispersions σ_v (σ_P in G98); (ii) the values of the “corrected” virial masses, M (M_{CV} in G98), contained within the radius $0.002 \cdot \sigma_v \cdot h^{-1} \text{ Mpc}$; (iii) the King-like galaxy number-density profile which is fitted for each cluster and used to rescale M at different radii. Hereafter, we limit our analysis to the 152 Abell-ACO clusters which span the wide interval of richness classes $-1 \leq R \leq 4$ (cf. Tab. 1 of G98), where the richness class $R = -1$ is assigned to clusters with Abell number counts $N_C < 30$ (Abell, Corwin, & Olowin 1989).

The G98 sample is complete neither in volume nor in richness. However, there exists a well defined, although rather scattered, correlation between cluster richness and mass. Indeed, in Table 1 we show that, although the cluster mass increases with richness, there is a large mass superposition between different richness classes R at a given mass. This is also explicitly shown in Figure 1, where we plot the mass distribution for different R classes. Mazure et al. (1996, § 6; M96 hereafter) showed that the remarkable scatter in the σ_v - R relation is largely intrinsic. The propagation of this scatter is the main reason for the scatter in the M - R relation since the relation between mass and σ_v is rather strict (with a scatter of $\sim 10\%$; see the upper panel of Figure 2). Therefore, we expect that the scatter in the M - R relation is also largely intrinsic, much like that in the σ_v - R relation.

TABLE 1

M VS. ABELL RICHNESS R

| R | Cluster # | $\log(M/M_\odot)$ |
|----------|-----------|-------------------|
| -1 | 7 | 14.08 ± 0.15 |
| 0 | 20 | 14.13 ± 0.10 |
| 1 | 74 | 14.24 ± 0.06 |
| 2 | 35 | 14.61 ± 0.08 |
| ≥ 3 | 7 | 14.74 ± 0.11 |

The 17 multipeaked clusters (see text) are not reported here.

In order to obtain a more representative cluster sample which also accounts for the presence of this scatter in

the M - R relation, we resample our clusters so as to mimic the R -distribution of the Edinburgh–Durham Cluster Catalogue (EDCC), which is claimed to be complete also for rather poor clusters (Lumsden et al. 1992). We compute the mass distribution by using 10,000 random extraction of the measured M values, distributed according to the EDCC R -distribution, by rescaling the EDCC richness to Abell’s (see also B93; Girardi et al. 1993; F96). The effectiveness of this resampling procedure has been shown by F96, who applied it to a sample similar to the G98 one in order to obtain the σ_v -distribution. As a result (cf. their Figure 6), they were able to reproduce the σ_v -distribution derived by M96 for the volume- and richness-complete ENACS sample, with the further advantage of extending the richness range from $R = 1$ to $R = -1$ and, therefore, the σ_v range of completeness from $\sigma_v \geq 800 \text{ km s}^{-1}$ down to $\sigma_v \geq 650 \text{ km s}^{-1}$.

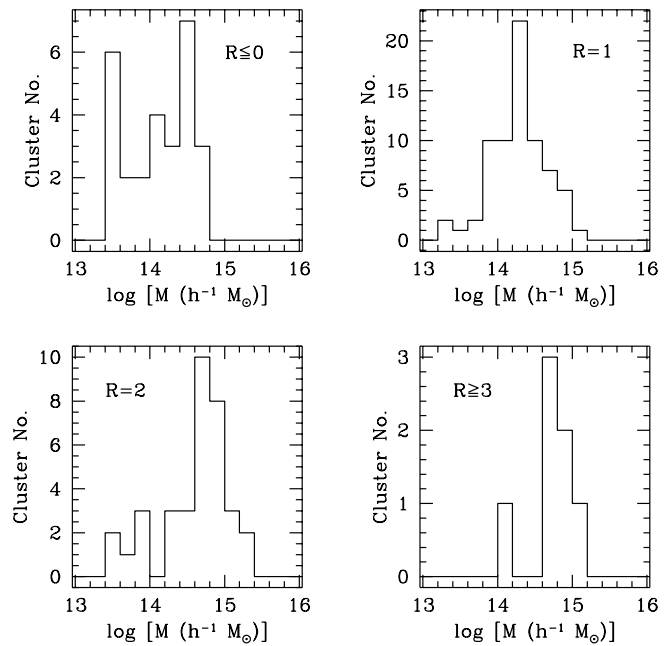


Fig. 1.— The mass distributions for clusters belonging to different richness classes. $R = 0$ and $R = -1$ classes are here considered together, owing to their similar mass distribution and to the small number of $R = -1$ clusters (see also text and Table 1).

In the present analysis, we apply the resampling procedure both to the whole sample of 152 $R \geq -1$ clusters and to the sample of 120 $R \geq 1$ clusters and obtain the corresponding mass distributions. Since no substantial difference exists between masses for $R = -1$ and $R = 0$ classes and owing to the small number of $R = -1$ clusters, we treat these two classes together. We verified that no difference is found in the final results if the two classes are instead treated separately.

Having determined the shape of the mass function

through this resampling procedure, we have still to fix its amplitude by resorting to an external normalization. To this purpose, we adopt the cluster volume density $\bar{N} = 8.6 \times 10^{-6} (h^{-1} \text{Mpc})^{-3}$ for $R \geq 1$ clusters, as provided by M96 for ENACS, scaled to the EDCC R -frequencies. Since the M96 value was corrected for the incompleteness of the Abell-ACO catalog with respect to the EDCC catalog, our normalization is consistent with the resampling procedure.

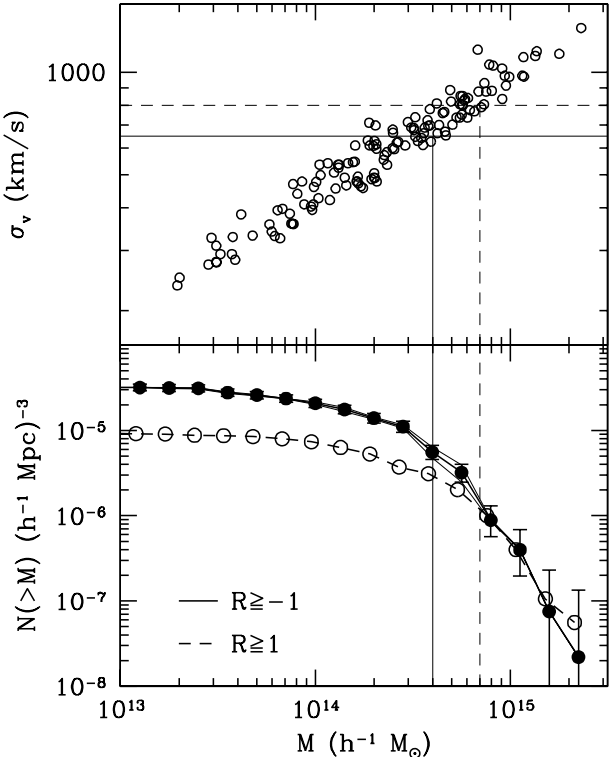


Fig. 2.— The lower panel shows the cumulative mass function for $R \geq -1$ clusters (filled points with solid line) and for $R \geq 1$ clusters (open points with dashed line). Error bars represent $1-\sigma$ uncertainties. The two curves above and below the $R \geq -1$ mass function correspond to two different ways in which clusters, which appear as multi-peaked in velocity space, are treated (see text). The mass completeness limits for the two richness classes (indicated by the vertical lines) are inferred from the relation between mass and velocity dispersion, as reported in the upper panel and from the corresponding σ_v completeness limits.

We estimate the mass-completeness limit in our sample from that in σ_v . The broad relation between richness and σ_v limits the completeness in velocity dispersion to $\sigma_v \geq 650 \text{ km s}^{-1}$ for a sample with $R \geq -1$ clusters (F96) and to $\sigma_v \geq 800 \text{ km s}^{-1}$ for the sample with $R \geq 1$ clusters (M96). Then, the less scattered $M-\sigma_v$ relation (see the upper panel of Figure 2) is used to estimate the mass completeness limit. We find $M \gtrsim 4 \times 10^{14} h^{-1} M_\odot$ for $R \geq -1$ and $M \gtrsim 7 \times 10^{14} h^{-1} M_\odot$ for $R \geq 1$.

In the lower panel of Figure 2 we show the resulting cumulative mass functions, $N(> M) = \int_M^\infty n(M) dM$ for

$R \geq -1$ clusters (filled points) and that for $R \geq 1$ clusters (open points). As expected, the curves flatten at small masses due to the effect of the incompleteness, while they are almost overlapping within the common completeness range. Errors in the mass function have been estimated by taking the contribution from (a) the Poissonian uncertainties from the finite statistics in the G98 sample; (b) the uncertainty in the resampling procedure connected with the Poissonian errors in the richness frequency distribution of the EDCC; (c) the uncertainties in the individual cluster mass estimates. In this plot and in the following, errorbars for the mass function correspond to the $1-\sigma$ overall errors contributed by such three sources.

The ambiguity in how to treat the 17 highly substructured clusters found in the sample give rise to two different determinations of the mass function, depending on whether each of them is treated as a single structure or as disjoined into two objects (cf. also § 6 in G98). The resulting mass functions for the $R \geq -1$ case are plotted in Figure 2 with the lower and upper light continuous lines, respectively. It turns out that they are always very close, the difference being within the statistical uncertainties. In the following we will refer to the $N(> M)$ plotted with the heavy solid line, which is computed by assigning equal weights to joined and disjoined peaks.

2.3 Comparison with Previous Estimates

In order to compare our optical virial mass function with those provided by BC93 and B93, we rescale our cluster mass estimates to the same $1.5 h^{-1} \text{Mpc}$ radius by using the fitted galaxy distributions (see the discussion in § 2.1) and recompute the mass function. The result of this comparison, which is plotted in Figure 3, shows that our mass function is intermediate between the two previous determinations. Following a maximum-likelihood approach, we find the following expression for our mass function:

$$n(M) = n^* \left(\frac{M}{M^*} \right)^{-1} e^{-M/M^*} \quad (1)$$

with $n^* = 2.6_{-0.4}^{+0.5} \times 10^{-5} (h^{-1} \text{Mpc})^{-3} (10^{14} h^{-1} M_\odot)^{-1}$ and $M^* = 2.6_{-0.6}^{+0.8} \times 10^{14} h^{-1} M_\odot$.

The mass function by B93 (upper panel of Figure 3) is based on cluster masses estimated from a homogeneous virial analysis and on the same resampling procedure that we followed here. Therefore, it is directly comparable to our results. Since B93 did not provide a normalization for their mass distribution, we fix it according to the $R \geq 1$ cluster number density provided by M96. The discrepancy with respect to B93 can be explained by the fact that the G98 mass estimates are on average 40% smaller than their estimates. This is explicitly shown by the dashed curve in the plot, which gives the mass function of B93 after just translating masses by 40% toward smaller values. As discussed in detail by G98 (cf. their § 8), two factors contribute to this difference. First, the more rigorous algorithm for removing interlopers gives a smaller σ_v by a factor of 10%, thus translating into a 20% difference in mass. Second, the use of the surface correction term in

the virial theorem (cf. § 2.1 and Carlberg et al. 1997b) decreases the mass estimate by about a further 20%.

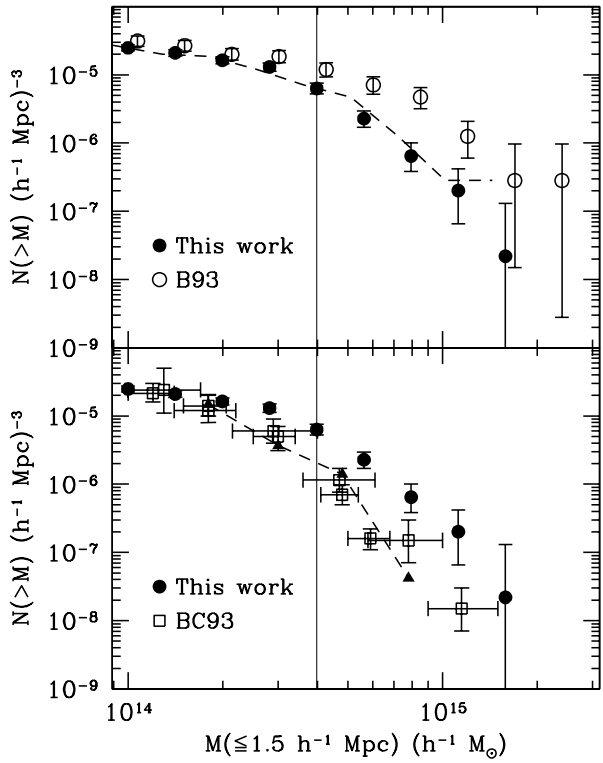


Fig. 3.— The comparison between this and previous determinations of $N(> M)$ by Biviano et al. (1993; upper panel) and by Bahcall & Cen (1993; lower panel; only their determination from optical cluster data is reported here). The vertical line in both panels indicates our limiting completeness mass. In the upper panel the dashed line indicates the B93 mass function after rescaling their masses by 40% to smaller values. In the lower panel the four triangles joined by a dashed line indicate the determination of $N(> M)$ we would have obtained from our sample by neglecting the scatter in the mass-richness relation (see text). The plotted errorbars for $N(> M)$ represent $1-\sigma$ uncertainties.

As for the optical data analysis by BC93, they associated the Abell or EDCC cluster richness to mass according to a suitable one-to-one scaling relation (cf. their eq. 4; note that this relation falls within the range, $M(\leq 1.5 h^{-1} Mpc) = (0.5 - 0.7) 10^{13} N_c$, that we find to hold for our cluster sample). The resulting $N(> M)$ turns out to be somewhat smaller than ours, the difference being larger at larger masses (cf. the lower panel of Figure 3). The main reason for this difference is due to the fact that the procedure by BC93 amounts to neglect any intrinsic scatter in the mass-richness relation (cf. § 2.2 about the necessity of accounting for this scatter). In order to show the effect of neglecting this scatter on the BC93 results, we consider the mass limits corresponding to the $R \geq 0$, $R \geq 1$, $R \geq 2$ and $R \geq 3$ clusters, according to the BC93 mass-richness relation. At these mass limits, we show the fractions of our resampled clusters (triangles connected by

a dashed line in the lower panel of Figure 3) corresponding to the four above richness ranges, when neglecting the contribution from poorer clusters. This shows the relevance of properly including the effect of the scatter in the M – R relation and by how much the mass function would have been underestimated without accounting for it.

In this context, the normalization is only a minor source of discrepancy between BC93 and our $N(> M)$ since they are comparable at very small masses ($\sim 1 - 2 \times 10^{14} h^{-1} M_\odot$) when the whole cluster sample is considered. However, we stress that, at the small mass values which are beyond our estimate of completeness limit, both BC93 and our $N(> M)$ neglect the significant contribution from the poor galaxy systems which are not recovered in Abell and EDCC catalogues.

3 IMPLICATIONS FOR COSMOLOGICAL MODELS

In order to compare our mass function to predictions of models for cosmic structure formation, we follow the Press–Schechter (1974, PS) approach, which provides the following expression for the number density of local clusters with mass in the range $[M, M + dM]$:

$$n(M) dM = \sqrt{\frac{2}{\pi}} \frac{\bar{\rho}}{M^2} \frac{\delta_c}{\sigma_M} \left| \frac{d \log \sigma_M}{d \log M} \right| \exp \left(-\frac{\delta_c^2}{2\sigma_M^2} \right) dM. \quad (2)$$

Here $\bar{\rho}$ is the average matter density and δ_c is the linear-theory overdensity for a uniform spherical fluctuation which is now collapsing; it is $\delta_c = 1.686$ for $\Omega_0 = 1$, with a weak dependence on Ω_0 for both flat and open geometries (e.g., Eke et al. 1996). The r.m.s. linear density fluctuation σ_M at the mass scale M is related to the fluctuation power spectrum according to $\sigma_M^2 = (2\pi^2)^{-1} \int_0^\infty dk k^2 P(k) W^2(kR)$. Here $W(x) = 3(\sin x - x \cos x)/x^3$ is the Fourier transform of the window function, assumed to have the top-hat profile. Accordingly, the mass M of a cluster arising from the collapse of a fluctuation with typical size R is $M = (4\pi/3)\bar{\rho}R^3$. The PS mass function has been compared with N-body simulations by several authors (e.g., Eke et al. 1996; Lacey & Cole 1996; Borgani et al. 1998; Gross et al. 1998) and has been generally shown to provide a rather accurate description of the abundance of virialized halos of cluster size.

Herebelow, we assume for the power spectrum of density fluctuations the expression $P(k) = A k T^2(k)$, where the transfer function is given by

$$T(q) = \frac{\ln(1 + 2.34q)}{2.34q} \times \\ \times [1 + 3.89q + (16.1q)^2 + (5.46q)^3 + (6.71q)^4]^{-1/4}, \quad (3)$$

with $q = k/\Gamma h$. This expression has been provided by Bardeen et al. (1986) for CDM models with negligible baryon contribution, once $\Gamma = \Omega_0 h$ is taken for the shape parameter. In the following, however, we will take Γ to be a free quantity to be fitted to observations, thus interpreting eq.(3) as a purely phenomenological expression for

the transfer function. As for the amplitude of the power-spectrum, it is customary to express it in terms of σ_8 , the r.m.s. fluctuation amplitude within a top-hat sphere of $8h^{-1} Mpc$ radius. Therefore, the class of models that we are considering is represented by three parameters, Ω_0 , Γ and σ_8 , either with or without a cosmological constant term, $\Omega_\Lambda = 1 - \Omega_0$, to provide flat spatial geometry. If we further require our model to satisfy the constraint provided by the four-year *COBE* data (see, e.g., Bunn & White 1997 and Hu & White 1997, for flat and open geometry, respectively), then we would have a one-to-one relation between the shape Γ and the amplitude σ_8 for each value of Ω_0 , thus reducing to two the number of free parameters.

The cluster mass which appears in the PS formula refers to the mass M_{vir} contained within the virialization radius R_{vir} , whose value depends on the cosmological parameters Ω_0 and Ω_Λ . Therefore, for the sake of comparison with PS predictions, the mass function presented in the § 2.2 should be suitably re-estimated model by model. If Δ_c is the ratio between the mean density within the virial radius and the critical average density, whose value depends on Ω_0 and Ω_Λ (e.g., Kitayama & Suto 1996; $\Delta_c = 18\pi^2 \simeq 178$ for $\Omega_0 = 1$), then $R_{vir}^3 = 3\Omega_0 M_{vir}/(4\pi\bar{\rho}\Delta_c)$. Therefore, the value of R_{vir} depends on M_{vir} , so that we resort to the following recursive procedure to compute it for each cluster. After taking the mass contained within the radius $0.002\sigma_v$ as a first guess for M_{vir} (cf. § 2.1), we (i) provide a new estimate of R_{vir} according to the above expression, and (ii) estimate the new M_{vir} by rescaling the previous value to the updated R_{vir} , using the appropriate cluster density profile (cf. § 2.1). We explicitly compute the observational mass function $n(M)$ for $\Omega_0 = 0.2, 0.4, 1$ for both open and flat models, while it is estimated by linear interpolation for intermediate Ω_0 values. In our analysis, we applied eq.(2) at $z = 0.05$, which represents the median redshift of the G98 cluster sample. In any case we find that, for the considered range of models, the mass function can always be well fitted by the parametric expression of eq.(1), with $M^* \simeq 3.5 \times 10^{14} h^{-1} M_\odot$ and normalization varying in a rather small range, $n^* \simeq (0.9 - 1.3) \times 10^{-5} (h^{-1} Mpc)^{-3} (10^{14} h^{-1} M_\odot)^{-1}$.

A further reason of caution when comparing data and model predictions on $n(M)$ is related to observational uncertainties in estimates of cluster masses, which are in general not negligible. G98 provides mass uncertainties by propagating statistical errors in the estimates of the velocity dispersion σ_v and of the virial radius (cf. col. 3. of Table 3 in G98). Such errors are correlated with cluster masses, being relatively smaller for richer, better sampled clusters. They range from $\sim 15\%$ at $M \simeq 2 \times 10^{15} h^{-1} M_\odot$ to $\sim 35\%$ at $M \simeq 10^{14} h^{-1} M_\odot$. Therefore, the measured mass function results from the convolution of the intrinsic $n(M)$ with mass errors. In order to account for them, we convolve the PS mass function of eq.(2) with the uncertainties in the mass estimates, as provided by G98.

We show in Figure 4 the observational $n(M)$, for $\Omega_0 = 0.4$ and $\Omega_\Lambda = 0.6$, in the mass range where the sample is

considered as complete (cf. § 2.2). Also plotted are the predictions for models with $\Omega_0 = 0.4$ and $\Omega_\Lambda = 0.6$, in order to show the effect of varying σ_8 and Γ separately (lower and upper panel, respectively). From the upper panel we show that $n(M)$ is rather insensitive to the shape of $P(k)$ (see, e.g., White et al. 1993), at least for $M \lesssim 10^{15} h^{-1} M_\odot$, where $n(M)$ is better determined. By varying Γ over a rather large range, much larger than that allowed by the power-spectrum of the observed galaxy distribution (e.g., Peacock & Dodds 1994), does not significantly change the goodness of the fit. On the contrary, our mass function represents a strong constraint for the amplitude of the power-spectrum (cf. the lower panel). The heavy and light curves in the lower panel show the PS predictions with and without convolving with mass uncertainties, respectively. Although the effect of such errors is never large, it turns out that at the smallest mass scale its size is of the same order of the error bar in the observational $n(M)$. Therefore, we prefer not to neglect it in our analysis.

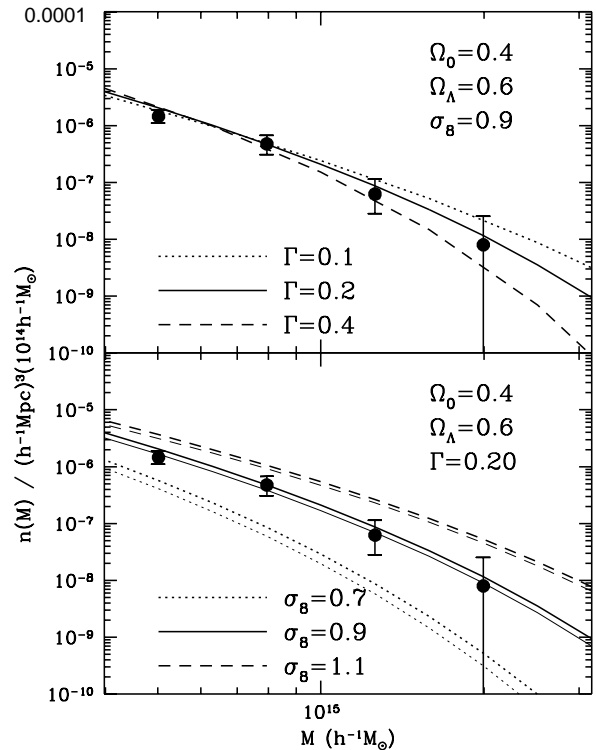


Fig. 4.— The effect of varying the power-spectrum shape parameter Γ (upper panel) and σ_8 (lower panel) on the error-convolved Press-Schechter mass function. Heavy and light curves in the lower panel are the PS mass function with and without convolving the model predictions with the uncertainties in the mass estimates. Filled dots represent the observational $n(M)$, with masses estimated within the virialization radius for a model with $\Omega_0 = 0.4$ and $\Omega_\Lambda = 0.6$.

If we impose the *COBE*-normalization, our observational $n(M)$ provides a relation between σ_8 and Ω_0 in the model parameter space. In order to estimate the confidence level for model rejection, we adopt a χ^2 -minimization procedure with respect to σ_8 (or, equiva-

lently, with respect to Γ) for each value of Ω_0 . The probability for a model to be accepted is then computed as the probability that the observed $n(M)$ comes from the parent model distribution with Gaussian random variations in logarithmic units given by the size of the error bars. As a result, we find that the 90% c.l. constraints on the σ_8 – Ω_0 plane can be represented by the fitting expressions

$$\begin{aligned}\sigma_8 &= (0.60 \pm 0.04) \times \Omega_0^{-0.46+0.09\Omega_0}; \Omega_\Lambda = 1 - \Omega_0 \\ \sigma_8 &= (0.60 \pm 0.04) \times \Omega_0^{-0.48+0.17\Omega_0}; \Omega_\Lambda = 0\end{aligned}\quad (4)$$

which are accurate within 2% in the range $0.2 \leq \Omega_0 \leq 1$. We note that these constraints come from the mass function estimated above the mass completeness limit which is appropriate for $R \geq -1$ clusters (cf. § 2.2). If, instead, we use the $R \geq 1$ mass completeness limit, $M_{lim} \simeq 7 \times 10^{14} h^{-1} M_\odot$, then we find $\sigma_8 = (0.62 \pm 0.08)$ for $\Omega_0 = 1$, with similar rescalings as in eq.(4) for $\Omega_0 < 1$. Our results are therefore unaffected by narrowing the completeness mass range. The only effect is that of increasing the uncertainties, due to the more limited mass range over which theoretical predictions are tested.

Our results can be compared with similar results obtained by other authors from the cluster abundance. White et al. (1993) obtained $\sigma_8 = 0.57 \pm 0.05$ for $\Omega_0 = 1$ from the median velocity dispersion of Abell clusters, as provided by Girardi et al. (1993), and from the temperature functions by Henry & Arnaud (1991) and Edge et al. (1990). Viana & Liddle (1996) obtained $\sigma_8 \simeq 0.6$ for $\Omega_0 = 1$ by fitting the cluster temperature function by Henry & Arnaud (1991) at 7 keV. A somewhat smaller normalization, $\sigma_8 = 0.52 \pm 0.04$ for $\Omega_0 = 1$, has been found by Eke et al. (1996), also based on the analysis of the cluster temperatures by Henry & Arnaud (1991) (see also Markevitch 1998, for a similar result based on recent ASCA temperature data). Oukbir, Bartlett & Blanchard (1997) found the same result as White et al. (1993), also from the X -ray temperature function. Borgani et al. (1998) obtained $\sigma_8 = 0.58 \pm 0.02$ for $\Omega_0 = 1$ from the local X -ray luminosity functions provided by Ebeling et al. (1997) and Rosati et al. (1998). It is remarkable that all such results, although based on largely different data sets are rather consistent with each other and converges to indicate that $\sigma_8 \simeq 0.6$ for $\Omega_0 = 1$, with rescalings for different Ω_0 values which are in general quite close to those in eq.(4).

4 CONCLUSIONS

In this paper we have presented a new determination of the mass function $n(M)$ of nearby galaxy clusters. This analysis is based on the virial mass estimates by Girardi et al. (1998, G98), for a sample of 152 Abell-ACO clusters which includes both data from the literature and the new ENACS data (Katgert et al. 1998). The extension of this sample, along with the good agreement found by G98 be-

tween optical and virial masses, makes it the largest data set over which to reliably estimate the local ($z \simeq 0.05$) cluster mass function.

The main results of our analysis can be summarized as follows.

- (a) After applying a suitable resampling procedure to account for the lack of volume- and richness-completeness of the G98 sample, $n(M)$ is reliably computed for masses larger than $M_{lim} \simeq 4 \times 10^{14} h^{-1} M_\odot$. At this mass limit, the value of the cumulative mass function is $N(> M) = (6.3 \pm 1.2) \times 10^{-6} (h^{-1} \text{Mpc})^{-3}$ for masses estimated within the $1.5 h^{-1} \text{Mpc}$ radius. The corresponding differential mass function is fitted with a Schechter-like function [cf. eq.(1)], with normalization $n^* = 2.6_{-0.4}^{+0.5} \times 10^{-5} (h^{-1} \text{Mpc})^{-3} (10^{14} h^{-1} M_\odot)^{-1}$ and characteristic mass $M^* = 2.6_{-0.6}^{+0.8} \times 10^{14} h^{-1} M_\odot$.
- (b) A comparison with previous mass function estimates, also based on optical data, by Biviano et al. (1993, B93) and Bahcall & Cen (1993, BC93), shows that our $n(M)$ is intermediate between these two, B93 and BC93 providing a larger and smaller estimate, respectively (cf. Figure 3).
- (c) A comparison with the predictions from models of cosmic structure formation demonstrates that our observational mass function provides a robust determination of the amplitude of the fluctuation power spectrum at the cluster mass scales (cf. Figure 4). After suitably convolving the prediction from the Press-Schechter (1974) mass function with the observational errors in the mass estimates, we determine σ_8 for COBE-normalized models with a $\sim 7\%$ uncertainty (at the 90% c.l.). It turns out that $\sigma_8 \simeq 0.6$ for $\Omega_0 = 1$, with appropriate rescalings at different Ω_0 values [cf. eqs.(4)].

As a concluding remark, we point out that a precise determination of $n(M)$ for local clusters, combined with a similar virial analysis of clusters at higher redshift, $z \simeq 0.3-0.5$, would provide information about the degree of evolution of the cluster abundance and, therefore, would allow one to estimate σ_8 and Ω_0 separately (see, e.g., Bahcall, Fan, & Cen 1997; Carlberg et al. 1997a). The implication of the mass function presented in this paper on the evolution of the cluster abundance will be discussed in detail in a future paper.

S.B. wish to acknowledge SISSA and Osservatorio Astronomico di Trieste for the hospitality during the preparation of this paper. This work has been partially supported by the Italian Ministry of University, Scientific Technological Research (MURST), by the Italian Space Agency (ASI).

REFERENCES

Abell, G. O., Corwin, H. G. Jr., & Olowin, R. P. 1989, *ApJS*, 70, 1

Allen, S. W. 1997, *MNRAS*, in press, preprint astro-ph/9710217

Bardeen, J. M., Bond, J. R., Kaiser, N., & Szalay, A., S., 1986, *ApJ*, 304, 15

Bahcall, N. A., & Cen, R. 1993, *ApJ*, 407, L49 (BC93)

Bahcall, N. A., Fan, X., & Cen, R. 1997, *ApJ*, 485, L53

Bahcall, N. A., & Lubin, L. M. 1994, *ApJ*, 426, 513

Binney, J., & Tremaine, S. 1987, in *Galactic Dynamics*, ed. J.P. Ostriker, Princeton University, Princeton University Press, New Jersey

Biviano, A., Girardi, M., Giuricin, G., Mardirossian, F., & Mezzetti, M. 1993, *ApJ*, 411, L13 (B93)

Borgani, S., Gardini, A., Girardi, M., & Gottlöber, S. 1997, *NewA*, 2, 119

Borgani, S., Rosati, P., Tozzi, P., & Norman, C. 1998, *ApJ*, submitted

Bower, R. G. 1997, *MNRAS*, 288, 355

Bryan, G. L., & Norman, M. L. 1998, *ApJ*, 495, 80

Bunn, E. F., & White, M. 1997, *ApJ*, 480, 6

Carlberg, R. G., Morris, S. L., Yee H. K. C., & Ellingson, E. 1997a, *ApJ*, 478, 462

Carlberg, R. G., Yee, H. K. C., & Ellingson, E. 1997b, *ApJ*, 479, L19

Carlberg, R. G., Yee, H. K. C., Ellingson, E., Morris, S. L., Abraham, R., Gravel, P., & Pritchett, C. J. 1997c, *ApJ*, 476, L7

Cavaliere, A., Menci, N. & Tozzi, P. 1997, *ApJ*, 484, L21

Cirimele, G., Nesci, R., & Trevese, D. 1997, *ApJ*, 475, 11

Durret, F., Gerbal, D., Lachieze-Rey, M., Lima-Nieto G., & Sadat, R. 1994, *A&A*, 287, 733

Ebeling, H., Edge, A. C., Fabian, A. C., Allen, S. W., Crawford, C. S., & Böhringer, H. 1997, *ApJ*, 479, L101

Edge, A. C., Stewart, G., Fabian, A. C., & Arnaud, K. A. 1990, *MNRAS*, 245, 559

Eke, V. R., Cole, S., & Frenk, C. S. 1996, *MNRAS*, 282, 263

Eke, V. R., Navarro, J. L., & Frenk, C. S. 1997, preprint astro-ph/9708070

Evrard, A. E., Metzler, C. A., & Navarro, J. F. 1996, *ApJ*, 469, 494

Fadda, D., Girardi, M., Giuricin, G., Mardirossian, F., & Mezzetti, M. 1996, *ApJ*, 473, 670 (F96)

Frenk, C. S., Evrard, A. E., White S. D. M., & Summers, F. J. 1996, *ApJ*, 472, 460

Frenk, C. S., White, S. D. M., Eftstathiou G., & Davis, M. 1990, *ApJ*, 351, 10

Girardi, M., Biviano, A., Giuricin, G., Mardirossian, F., & Mezzetti, M. 1993, *ApJ*, 404, 38

Girardi, M., Biviano, A., Giuricin, G., Mardirossian, F., & Mezzetti, M. 1995, *ApJ*, 438, 527

Girardi, M., Fadda, D., Escalera, E., Giuricin, G., Mardirossian, F., & Mezzetti, M. 1997, *ApJ*, 490, 56

Girardi, M., Giuricin, G., Mardirossian, F., Mezzetti, M., & Boschin W. 1998, *ApJ*, in press, preprint astro-ph/9804187 (G98)

Giuricin, G., Mardirossian, F., & Mezzetti, M. 1982, *ApJ*, 255, 361

Gross, M. A. K., Somerville, R. S., Primack, J. R., Borgani, S., & Girardi, M. 1998, in preparation

Henry, J. P., & Arnaud, K. A. 1991, *ApJ*, 372, 410

Hu, W., & White, M. 1997, *ApJ*, 486, L1

Katgert, P., Mazure, A., den Hartog, R., Adami, C., Biviano, A., & Perea, J. 1998, *A&AS*, 129, 399

Katgert, P., et al. 1996, *A&A*, 310, 8

Kitayama, T., & Suto, Y. 1996, *ApJ*, 469, 480

Lacey, C. G., & Cole, S. 1993, *MNRAS*, 262, 627

Limber, D. N., & Mathews, W. G. 1960, *ApJ*, 132, 286

Lumsden, S. L., Nichol, R. C., Collins, C. A., & Guzzo, L. 1992, *MNRAS*, 258, 1

Makino, N., Sasaki, S., & Suto, Y. 1998, *ApJ*, 497, 555

Markevitch, M. 1998, *ApJ*, in press, preprint astro-ph/9802059

Mazure, A., et al. 1996, *A&A*, 310, 31 (M96)

Merritt, D. 1988, in *The Minnesota lectures on clusters of galaxies and large-scale structure* (San Francisco: Astronomical Society of the Pacific) p. 175-196.

Merritt, D., & Tremblay, B. 1994, *AJ*, 108, 514

Narayan, R., & Bartelmann, M. 1997, in *Formation of Structure in the Universe*, eds. A. Dekel and J.P. Ostriker (Cambridge University Press), preprint astro-ph/9606001

Oukbir, J., Bartlett, J. G., & Blanchard A. 1997, *A&A*, 320, 365

Peacock, J. A., & Dodds, S. J. 1994, *MNRAS*, 267, 1020

Press, W. H., & Schechter, P. 1974, *ApJ*, 187, 425 (PS)

Rosati, P., Della Ceca, R., Norman, C., & Giacconi, R. 1998, *ApJ*, 492, L21

Schindler, S. 1996, *A&A*, 305, 756

The, L. S., & White, S. D. M. 1986, *AJ*, 92, 1248

van Haarlem, M. P., Frenk, C. S., & White, S. D. M. 1997, *MNRAS*, 287, 817

Viana, P. T. P., & Liddle, A. W. 1996, *MNRAS*, 281, 323

Watt, M. P., Ponman, T. J., Bertram, D., Eyles, C. J., Skinner, G. K., & Willmore, A. P. 1992, *MNRAS*, 258, 738

White, S. D. M., Efstathiou, G., & Frenk, C. S. 1993, *MNRAS*, 262, 1023

Wu, X. P., & Fang, L. Z. 1997, *ApJ*, 483, 62